JACS
JOURNAL OF THE AMERICAN CHEMICAL SOCIETY
Communication
pubs.acs.org/JACS

Emergence of the Dirac Electron System in a Single-Component Molecular Conductor under High Pressure

Reizo Kato,*[,†] HengBo Cui,[†] Takao Tsumuraya,[†,‡] Tsuyoshi Miyazaki,[§] and Yoshikazu Suzumura[∥]

[†]Condensed Molecular Materials Laboratory, RIKEN, Wako-shi, Saitama 351-0198, Japan
[‡]International Center for Young Scientists (ICYS), National Institute for Materials Science, Tsukuba 305-0044, Japan
[§]International Center for Materials Nanoarchitectonics (MANA), National Institute for Materials Science, Tsukuba 305-0044, Japan
[∥]Department of Physics, Nagoya University, Chikusa-ku, Nagoya 464-8602, Japan

Supporting Information

ABSTRACT: Single-component molecular conductors can provide a variety of electronic states. We demonstrate here that the Dirac electron system emerges in a single-component molecular conductor under high pressure. First-principles density functional theory calculations revealed that Dirac cones are formed in the single-component molecular conductor $[Pd(dddt)_2]$ (dddt = 5,6-dihydro-1,4-dithiin-2,3-dithiolate), which shows temperature-independent resistivity (zero-gap behavior) at 12.6 GPa. The Dirac cone formation in $[Pd(dddt)_2]$ can be understood by a tight-binding model. The Dirac points originate from the HOMO and LUMO bands, each of which is associated with different molecular layers. Overlap of these two bands provides a closed intersection at the Fermi level (Fermi line) if there is no HOMO−LUMO coupling. Two-step HOMO−LUMO couplings remove the degeneracy on the Fermi line, resulting in gap formation. The Dirac cones emerge at the points where the Fermi line intersects with a line on which the HOMO−LUMO coupling is zero.

Since the discovery of the ambient-pressure single-component molecular metal with a well-defined Fermi surface in 2001,[1] many neutral molecules have been surveyed to find exotic electronic states. Single-component molecular conductors belong to a multiple band system where both the HOMO and the LUMO in the same molecule contribute to the formation of conduction bands. The basic idea is an electron transfer from the HOMO-based band to the LUMO-based band, leading them to a partially filled state. In most single-component molecular crystals, these bands are separated from each other at ambient pressure, which leads to insulating properties. The application of pressure, however, enlarges the bandwidth of each band and induces overlap of them, which produces charge carriers. We are studying the pressure effect in single crystals of neutral metal−dithiolene complexes using a diamond anvil cell (DAC).[2] Metal−dithiolene complexes are known to have a small HOMO−LUMO energy gap and thus are suitable for the formation of the metallic band structure.[3] Indeed, we found that neutral $[Ni(dmit)_2]$ (dmit = 1,3-dithiole-2-thione-4,5-dithiolate), one of the most significant and fundamental components of molecular metals and superconductors, turns into a metal with a three-dimensional Fermi surface[4] and that neutral $[Ni(hfdt)_2]$ (hfdt = bis(trifluoromethyl)tetrathiafulvalenedithiolate) shows superconductivity under pressure.[5]

The Dirac cone, where the occupied band contacts the unoccupied band at a point in the wavenumber space, is known to induce exotic transport properties. The linear dispersion around the contact point realizes "massless Dirac fermions". Although the Dirac electron system has been reported to emerge in several systems, including graphene,[6] organic materials,[7] and edge states of topological insulators,[8] the number of Dirac electron systems in bulk crystals is still limited. In the course of a study of the pressure effect in the neutral metal−dithiolene complexes, we have found a Dirac electron system in $[Pd(dddt)_2]$ (dddt = 5,6-dihydro-1,4-dithiin-2,3-dithiolate) under high pressure. The $[Pd(dddt)_2]$ molecule, in which the central C═C double bond in the organic donor molecule bis(ethylenedithio)tetrathiafulvalene (BEDT-TTF) is replaced by a Pd ion, is known to provide various conducting cation radical salts.[9] We present here the resistivity under high pressure, crystal structure analysis, and band structure calculations for the neutral $[Pd(dddt)_2]$ crystal.

Neutral $[Pd(dddt)_2]$ crystals were prepared by oxidation of $[(n\text{-}Bu)_4N][Pd(dddt)_2]$ by I_2 in acetone and acetic acid according to the synthesis of $[Ni(dddt)_2]$.[10] Figure 1 shows

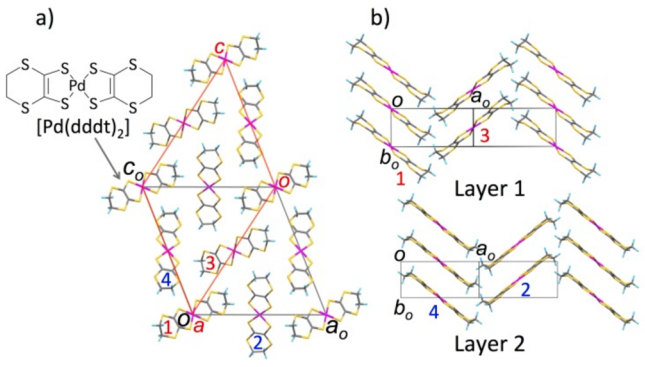

Figure 1. (a) Unit cell of $[Pd(dddt)_2]$. (b) Two crystallographically independent molecular layers.

Received: November 26, 2016
Published: January 25, 2017

DOI: 10.1021/jacs.6b12187
J. Am. Chem. Soc. 2017, 139, 1770−1773

the crystal structure of $[Pd(dddt)_2]$. The crystal belongs to the monoclinic system. The unit cell contains four molecules, and two of them (molecules 1 and 2) are crystallographically independent. Almost-planar molecules stack uniformly along the b axis. Along the diagonal **a** + **c** direction, the molecules show a corrugated arrangement, and crystallographically equivalent molecules form two kinds of layers, layer 1 (molecules 1 and 3) and layer 2 (molecules 2 and 4).

The temperature-dependent direct-current resistivity was measured under pressure using a DAC.[2] Electrical contacts were obtained by attaching four 10 μm gold wires with gold paint. The sample and wires were protected by a mixture of alumina and Araldite, resulting in a high success rate and high-quality hydrostatic pressure. The pressure medium was Daphne 7373 oil. The pressure was determined by the shift in the ruby fluorescence R1 lines at room temperature. At ambient pressure, the system was too insulating for the resistivity to be measured. The application of pressure decreased the resistivity and activation energy (Figure 2). The continuous

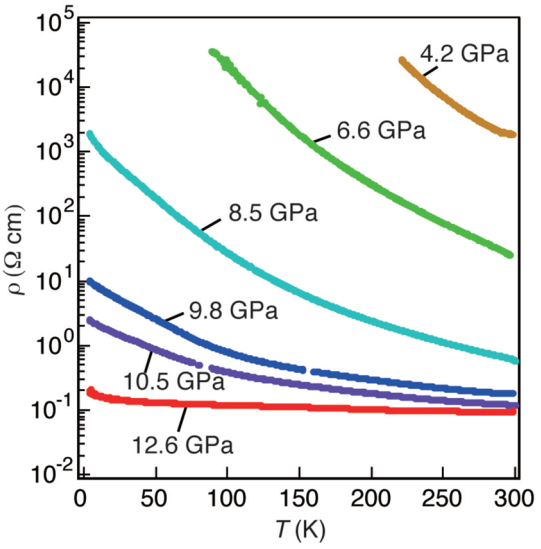

Figure 2. Temperature-dependent resistivity of $[Pd(dddt)_2]$ up to 12.6 GPa.

change in the resistivity behavior under pressure suggests the absence of a pressure-induced structural transition. At 12.6 GPa, the resistivity hardly changes over almost all of the temperature range. This almost-constant resistivity is surprising. Previous works, however, have shown that such constant resistivity in Dirac electron systems may be possible in the presence of a high density of scattering centers.[6,11]

We carried out first-principles density functional theory (DFT) calculations with the PW91 generalized gradient approximation (GGA)[12] to understand the high-pressure crystal and electronic structures. Using plane-wave basis sets with the ultrasoft pseudopotential technique,[13,14] we optimized the cell parameters as well as the internal coordinates of $[Pd(dddt)_2]$ at several hydrostatic pressures. Hereafter, for convenience in later discussions, we select a new a axis parallel to layer 1 and layer 2 and define a new cell as $\mathbf{a} = -(\mathbf{a}_o + \mathbf{c}_o)$, $\mathbf{b} = -\mathbf{b}_o$, $c = c_o$, where $\mathbf{a}_o$, $\mathbf{b}_o$, and $\mathbf{c}_o$ are the original lattice vectors (Figure 1).

The calculated HOMO−LUMO energy gap of an isolated molecule (Δ) is 0.65 eV, which is much smaller than that of ordinary π molecules (e.g., 1.67 eV for BEDT-TTF; see the Supporting Information (SI)). Since the unit cell contains four molecules, there are four HOMO-based bands and four LUMO-based bands. At ambient pressure, the system is a band insulator in which the fully occupied HOMO bands are separated from the unoccupied LUMO bands by a band gap of 0.22 eV (Figure S3). With increasing pressure, both the HOMO and LUMO bands become wider, and they overlap at 8 GPa (Figure 3a). The most remarkable feature of the energy

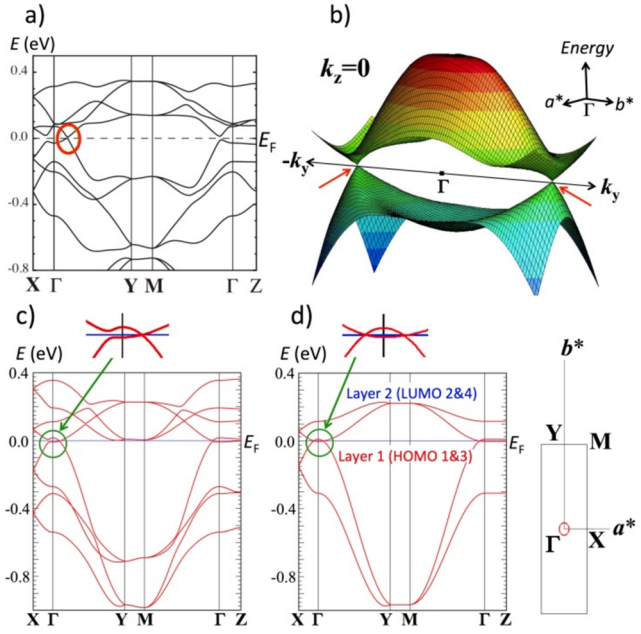

Figure 3. (a) Band structure at 8 GPa obtained by DFT calculations. (b) Dirac cones are indicated by red arrows. (c) Band structure obtained using the tight-binding model. (d) Band structure and Fermi surface obtained using the 4 × 4 matrix (see the text).

band structure at 8 GPa is the emergence of a pair of Dirac cones on the b^* axis (Figure 3b). This is consistent with the zero-gap behavior observed in the resistivity measurement. Because first-principles calculations based on the GGA usually underestimate the energy gap between the valence and conduction bands, it is reasonable that the calculated pressure needed to realize the zero-gap state is lower than the experimentally observed one.[15] The present result is the first case where the Dirac electron system emerges in a single-component molecular conductor. Notably, a pair of Dirac points emerges from the Γ point by the application of pressure.[16]

In order to understand the Dirac cone formation in this single-component system, we studied a tight-binding model based on extended Hückel molecular orbital calculations.[17] In the first step, we calculated overlap integrals between frontier molecular orbitals using the structural data optimized by the DFT calculation. The transfer integral is obtained by multiplying the overlap integral by a constant (−10 eV). Table 1 shows transfer integrals (HOMO−HOMO, LUMO−LUMO, and HOMO−LUMO) at 8 GPa. The transfer integrals can be categorized as those within layer 1 and layer 2 and the interlayer ones. In each layer, the largest transfer integrals are those along the stacking direction (b_1 and b_2). There also exist significant interstack transfer integrals (p in layer 1 and q in layer 2). The existence of the interlayer transfer integrals (a and c) indicates that the system has a three-dimensional character.

DOI: 10.1021/jacs.6b12187
J. Am. Chem. Soc. 2017, 139, 1770−1773

Table 1. HOMO−HOMO (H), LUMO−LUMO (L), and HOMO−LUMO (HL) Transfer Integrals (in meV) at 8 GPa

	H	L	HL	
b_1	204.0	64.8	21.9	
$p_1(p)$	39.8	20.5	-27.5	Layer 1
p_2	—	—	-29.3	
b_2	76.2	-41.3	-53.1	
$q_1(q)$	24.7	14.8	-18.6	Layer 2
q_2	—	—	-19.1	
a	-34.5	0	26.0	Interlayer
c	11.8	-16.7	21.8	

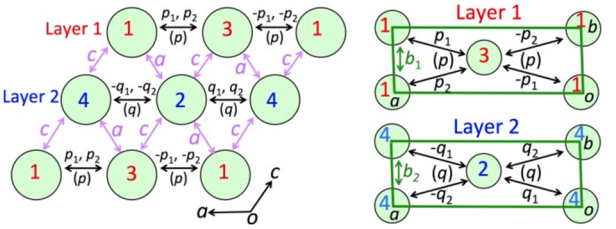

In the tight-binding model, we consider four $[Pd(dddt)_2]$ molecules (1, 2, 3, and 4; Figure 1) with HOMO ($H1$, $H2$, $H3$, $H4$) and LUMO ($L1$, $L2$, $L3$, $L4$) frontier molecular orbitals in the unit cell. The band energies $E(\mathbf{k})$ are obtained as eigenvalues of the following 8 × 8 Hermite matrix:

$$\hat{\mathbf{H}}(\mathbf{k}) = \begin{pmatrix} t_{H1,H1} & t_{H1,H2} & t_{H1,H3} & t_{H1,H4} & t_{H1,L1} & t_{H1,L2} & t_{H1,L3} & t_{H1,L4} \\ * & t_{H2,H2} & t_{H2,H3} & t_{H2,H4} & t_{H2,L1} & t_{H2,L2} & t_{H2,L3} & t_{H2,L4} \\ * & * & t_{H3,H3} & t_{H3,H4} & t_{H3,L1} & t_{H3,L2} & t_{H3,L3} & t_{H3,L4} \\ * & * & * & t_{H4,H4} & t_{H4,L1} & t_{H4,L2} & t_{H4,L3} & t_{H4,L4} \\ * & * & * & * & t_{L1,L1} & t_{L1,L2} & t_{L1,L3} & t_{L1,L4} \\ * & * & * & * & * & t_{L2,L2} & t_{L2,L3} & t_{L2,L4} \\ * & * & * & * & * & * & t_{L3,L3} & t_{L3,L4} \\ * & * & * & * & * & * & * & t_{L4,L4} \end{pmatrix}$$

where the matrix element $t_{\alpha,\beta}$ (given in the SI) is associated with the coupling between frontier molecular orbitals α and β and the symbol * expresses the complex conjugate (hereafter, we treat the complex conjugate implicitly).

The obtained energy band structure (Figure 3c) reproduces essential features of the one obtained by the first-principles calculation. In particular, the emergence of the Dirac points on the b^* axis strongly suggests that we can explain the formation of the Dirac cones using the tight-binding model. In order to assign molecular orbitals that contribute to the Dirac cone formation, we extracted the following 4 × 4 matrix:

$$\hat{\mathbf{H}}'(\mathbf{k}) = \begin{pmatrix} t_{H1,H1} & t_{H1,H3} & t_{H1,L2} & t_{H1,L4} \\ * & t_{H3,H3} & t_{H3,L2} & t_{H3,L4} \\ * & * & t_{L2,L2} & t_{L2,L4} \\ * & * & * & t_{L4,L4} \end{pmatrix}$$

The band structure given by the above matrix (Figure 3d) suggests that the Dirac points are associated with HOMOs in layer 1 ($H1$ and $H3$) and LUMOs in layer 2 ($L2$ and $L4$). A serious difference, however, is that the Dirac point is absent and the system has a two-dimensional Fermi surface, as shown in Figure 3d. This is because all of the off-diagonal matrix elements associated with direct HOMO−LUMO couplings in $\hat{\mathbf{H}}'(\mathbf{k})$ are zero ($t_{H1,L2} = t_{H1,L4} = t_{H3,L2} = t_{H3,L4} = 0$). If there are only intrastack HOMO−HOMO and LUMO−LUMO coupling elements ($t_{H1,H1} = t_{H3,H3} = 2b_{1H}\cos(\boldsymbol{kb})$ and $t_{L2,L2} = t_{L4,L4} = \Delta + 2b_{2L}\cos(\boldsymbol{kb})$), this 4 × 4 model has one-dimensional HOMO and LUMO bands, each of which is doubly degenerate. As a result of the opposite signs of the transfer integrals (b_{1H} and b_{2L}), the HOMO band is convex and the LUMO band is concave around the Γ point. The interstack HOMO−HOMO and LUMO−LUMO coupling elements ($t_{H1,H3}$ and $t_{L2,L4}$) containing transfer integrals p_H and q_L make each band split into two, and the upper HOMO band and the lower LUMO band cross each other (Figure 3d), which results in the formation of the two-dimensional Fermi surface. If there are HOMO−LUMO couplings, an energy gap opens at the crossing points and the Fermi surface disappears.[3] This is what happens in the original 8 × 8 model. However, $\hat{\mathbf{H}}'(\mathbf{k})$ with no direct HOMO−LUMO coupling cannot induce the band repulsion. This suggests that the original 8 × 8 matrix $\hat{\mathbf{H}}(\mathbf{k})$ contains indirect couplings between HOMOs in layer 1 ($H1$ and $H3$) and LUMOs in layer 2 ($L2$ and $L4$).

We examined the band structure of the 8 × 8 tight-binding model in which the intralayer HOMO−LUMO coupling elements are artificially set to zero ($t_{H1,L3} = t_{H3,L1} = t_{H2,L4} = t_{H4,L2} = 0$). In this case, the Dirac cones are absent, and the closed Fermi surface appears around the Γ point (Figure S4a). Similar emergence of the Fermi surface is also observed when the interlayer HOMO−HOMO and LUMO−LUMO coupling elements ($t_{H1,H2}$, $t_{H1,H4}$, $t_{H2,H3}$, $t_{H3,H4}$, $t_{L1,L4}$, and $t_{L2,L3}$) containing transfer integrals a_H, c_H, and c_L are assumed to be zero (Figure S4b). These results indicate that the gap opening originates from two-step couplings between HOMOs in layer 1 ($H1$ and $H3$) and LUMOs in layer 2 ($L2$ and $L4$), a product of the intralayer HOMO−LUMO and interlayer HOMO−HOMO/LUMO−LUMO couplings (Figure 4). For example, $H1$ interacts with $L2$ via $L3$ or $H4$. In general, the two-step HOMO−LUMO couplings can be understood by second-order perturbation theory (see the SI). Nevertheless, there exist points where the band repulsion does not act and the band crossing remains, which results in Dirac cone formation. This is the case because there is a line on which the HOMO−LUMO coupling is zero, and the Dirac cones emerge at the points where the line crosses the Fermi surface (line). Indeed, for every intralayer HOMO−LUMO coupling element ($t_{H1,L3}$, $t_{H3,L1}$, $t_{H2,L4}$, and $t_{H4,L2}$) there exists a line on which its value is zero in the wavenumber space, and all of these lines run along the Γ−Y line near the Γ point (Figure 5). This is consistent with the emergence of the Dirac cones on the Γ−Y line. A similar mechanism was discussed for the Dirac electron system in the cubic inverse perovskite Ca_3PbO and its family.[18] A point that differs from the Ca_3PbO system is the gap formation by the two-step HOMO−LUMO couplings.

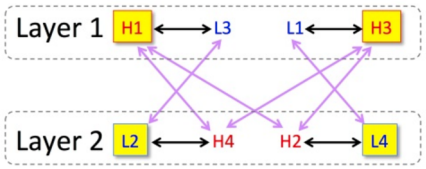

Figure 4. Two-step couplings between HOMOs in layer 1 ($H1$ and $H3$) and LUMOs in layer 2 ($L2$ and $L4$).

DOI: 10.1021/jacs.6b12187
J. Am. Chem. Soc. 2017, 139, 1770−1773

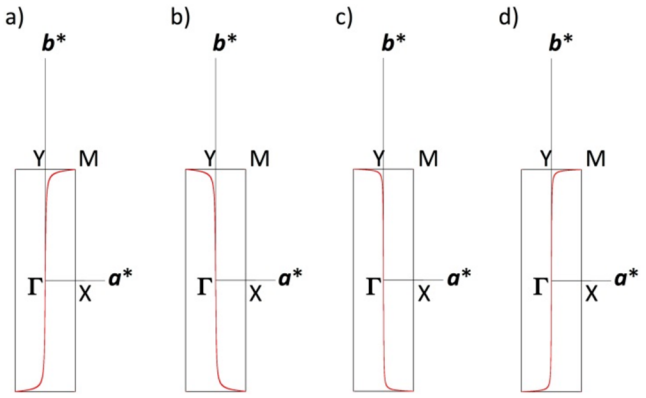

Figure 5. Lines on which the intralayer HOMO−LUMO coupling element is zero within the a^*b^* plane ($k_z = 0$): (a) $t_{H1,L3} = 0$; (b) $t_{H3,L1} = 0$; (c) $t_{H4,L2} = 0$; (d) $t_{H2,L4} = 0$.

In summary, we performed high-pressure resistivity measurements using a DAC and first-principles DFT band calculations for the single-component molecular conductor $[Pd(dddt)_2]$ and found that the Dirac electron system emerges under high pressure. A possible mechanism for the Dirac cone formation has been proposed using the tight-binding model. This is the first step to full understanding of this unique Dirac electron system. Details of the first-principles DFT calculations and the property of parity of the wave function at the time-reversal-invariant momentum will be reported elsewhere.

■ ASSOCIATED CONTENT

Supporting Information

The Supporting Information is available free of charge on the ACS Publications website at DOI: 10.1021/jacs.6b12187.

Crystal data at ambient pressure (CIF)
Supporting synthetic and theoretical information (PDF)

■ AUTHOR INFORMATION

Corresponding Author

*reizo@riken.jp

ORCID

Reizo Kato: 0000-0002-2606-4657

Notes

The authors declare no competing financial interest.

■ ACKNOWLEDGMENTS

The first-principles calculations in this study were performed on the Numerical Materials Simulator at the National Institute for Materials Science. The authors thank H. Kino (NIMS) and H. Seo (RIKEN) for their help in the theoretical part. This work was supported by the WPI Initiative on Materials Nanoarchitectonics of the Ministry of Education, Culture, Sports, Science and Technology of Japan. This work was supported by JSPS KAKENHI Grants JP16K17756, JP15H02108, JP 26400355, and JP16H06346.

■ REFERENCES

(1) Tanaka, H.; Okano, Y.; Kobayashi, H.; Suzuki, W.; Kobayashi, A. *Science* **2001**, *291*, 285.
(2) Cui, H. B.; Brooks, J.; Kobayashi, A.; Kobayashi, H. *J. Am. Chem. Soc.* **2009**, *131*, 6358.
(3) Kobayashi, A.; Fujiwara, E.; Kobayashi, H. *Chem. Rev.* **2004**, *104*, 5243.
(4) Cui, H. B.; Tsumuraya, T.; Miyazaki, T.; Okano, Y.; Kato, R. *Eur. J. Inorg. Chem.* **2014**, *2014*, 3837.
(5) Cui, H. B.; Kobayashi, H.; Ishibashi, S.; Sasa, M.; Iwase, F.; Kato, R.; Kobayashi, A. *J. Am. Chem. Soc.* **2014**, *136*, 7619.
(6) Novoselov, K. S.; Geim, A. K.; Morozov, S. V.; Jiang, D.; Katsnelson, M. I.; Grigorieva, I. V.; Dubonos, S. V.; Firsov, A. A. *Nature* **2005**, *438*, 197.
(7) (a) Tajima, N.; Tamura, M.; Nishio, Y.; Kajita, K.; Iye, Y. *J. Phys. Soc. Jpn.* **2000**, *69*, 543. (b) Katayama, S.; Kobayashi, A.; Suzumura, Y. *J. Phys. Soc. Jpn.* **2006**, *75*, 054705. (c) Mizuno, A.; Shuku, Y.; Suizu, R.; Matsushita, M. M.; Tsuchiizu, M.; Mañeru, D. R.; Illas, F.; Robert, V.; Awaga, K. *J. Am. Chem. Soc.* **2015**, *137*, 7612.
(8) Qi, X.-L.; Zhang, S.-C. *Rev. Mod. Phys.* **2011**, *83*, 1057.
(9) (a) Kushch, L. A.; Konovalikhin, S. V.; Buravov, L. I.; Khomenko, A. G.; Shilov, G. V.; Van, K.; Dyachenko, O. A.; Yagubskii, B.; Rovira, C.; Canadell, E. *J. Phys. I* **1996**, *6*, 1555. (b) Yagubskii, E. B.; Kushch, L. A.; Gritsenko, V. V.; Dyachenko, O. A.; Buravov, L. I.; Khomenko, A. G. *Synth. Met.* **1995**, *70*, 1039. (c) Kushch, L. A.; Yagubskii, E. B.; Konovalikhin, S. V.; Shilov, G. V.; Atovmyan, L. O. *Russ. Chem. Bull.* **1999**, *48*, 1513.
(10) Kim, H.; Kobayashi, A.; Sasaki, Y.; Kato, R.; Kobayashi, H. *Bull. Chem. Soc. Jpn.* **1988**, *61*, 579.
(11) (a) Shon, N. H.; Ando, T. *J. Phys. Soc. Jpn.* **1998**, *67*, 2421. (b) Tajima, N.; Sugawara, S.; Tamura, M.; Kato, R.; Nishio, Y.; Kajita, K. *Europhys. Lett.* **2007**, *80*, 47002.
(12) Perdew, J. P.; Wang, Y. *Phys. Rev. B: Condens. Matter Mater. Phys.* **1992**, *45*, 13244.
(13) Vanderbilt, D. *Phys. Rev. B: Condens. Matter Mater. Phys.* **1990**, *41*, 7892.
(14) Miyazaki, T.; Ohno, T. *Phys. Rev. B: Condens. Matter Mater. Phys.* **2003**, *68*, 035116.
(15) Tran, F.; Blaha, P. *Phys. Rev. Lett.* **2009**, *102*, 226401.
(16) Montambaux, G.; Piéchon, F.; Fuchs, J.-N.; Goerbig, M. O. *Phys. Rev. B: Condens. Matter Mater. Phys.* **2009**, *80*, 153412.
(17) Mori, T.; Kobayashi, A.; Sasaki, Y.; Kobayashi, H.; Saito, G.; Inokuchi, H. *Bull. Chem. Soc. Jpn.* **1984**, *57*, 627.
(18) Kariyado, T.; Ogata, M. *J. Phys. Soc. Jpn.* **2011**, *80*, 083704.

DOI: 10.1021/jacs.6b12187
J. Am. Chem. Soc. 2017, 139, 1770−1773